Physica B 173 (1991) 357–385
North-Holland

Molecular dynamics computer simulation of non-linear optical effects; electric polarisation due to optical rectification in a circularly polarised laser

M.W. Evans[1], G. Wagnière and S. Woźniak[2]

Institute of Physical Chemistry, University of Zurich, Winterthurerstrasse 190, CH-8057 Zurich, Switzerland

Received 1 February 1991
Revised manuscript received 26 April 1991

The technique of field applied molecular dynamics computer simulation is used to investigate the picosecond molecular dynamics of static and dynamic electric polarisation due to a laser field. A pulse of intense, circularly polarised, electromagnetic radiation is applied to a sample of chiral molecules and the molecular dynamics analysed statistically with time correlation functions computed in the presence of the laser. The effect of the laser on the molecular dynamics was animated and analysed visually. These dynamics measure the interaction between the imaginary part of the dynamic electronic polarisability and the conjugate product $\boldsymbol{\Pi}^{\wedge}$ of the laser. When the laser frequency is tuned to the THz region (corresponding to picosecond time scales of the natural molecular dynamics) the computer simulation shows the presence of frequency dependent magnetisation, measured by the $t \rightarrow \infty$ level of the component of the angular momentum correlation function in the axis of propagation of the laser. In general, the details of the molecular dynamic response are very sensitive to the frequency and intensity of the laser.

1. Introduction

Intense electromagnetic radiation produces a rich variety of non-linear effects in a molecular ensemble. "Non-linear" in this context refers to the functional dependence of the experimental observable on the electric field strength ($\boldsymbol{E}$ in volts/m) and the magnetic flux density ($\boldsymbol{B}$ in tesla) of the applied electromagnetic field (an intense laser beam). The inverse Faraday effect, for example, is magnetisation due to a circularly polarised laser, and was first predicted theoretically by Pershan [1]. It was later measured by Pershan and co-workers [2, 3] to be about 0.01 A/m for an intensity of about 10^{11} W/m^2. Further theoretical work was reported by Atkins and Miller [4], and the effect is briefly described in textbooks by Shen [5] and Atkins [6]. The methods used by Woźniak and co-workers [7–9] based on molecular property tensor methodology developed by the Kielich school [10] can also be used as a description of the inverse Faraday and related non-linear optical effects [11]. Recently, Wagnière [12] has provided a clear comparative analysis of the inverse Faraday effect, together with analytical expressions in diamagnetic and paramagnetic materials [13] from quantum perturbation theory. Feynman diagram analysis by Wagnière [13] and symmetry analyses by Evans [14–16] have placed it in the context of several other related non-linear optical effects, at increasing order in $\boldsymbol{E}$ and $\boldsymbol{B}$. Among these [13] is inverse magnetochiral birefringence; and "dynamic polarisation", introduced by Evans and

[1] Permanent address: 433 Theory Center, Cornell University, Ithaca, NY 14853, USA.
[2] Permanent address: Institute of Physics, A. Mickiewicz University, 60–780 Poznań, Poland.

0921-4526/91/$03.50

Wagnière [17]. The latter is electric polarisation due to optical rectification in a laser, and is investigated in this paper with field applied molecular dynamics computer simulation [18–20].

The original paper by Pershan [1] defines the inverse Faraday effect in terms of the conjugate product

$$\boldsymbol{\Pi}^{\mathrm{A}} = -\boldsymbol{E}_{\mathrm{L}}^{+} \times \boldsymbol{E}_{\mathrm{L}}^{-} = \boldsymbol{E}_{\mathrm{R}}^{+} \times \boldsymbol{E}_{\mathrm{R}}^{-} = -2E_0^2 \, \mathrm{i}\boldsymbol{e}_z \tag{1}$$

of a circularly polarised laser. Here L and R denote left and right circularly polarised light, respectively, and [13]

$$\boldsymbol{E}_{\mathrm{L}}^{\mp} = E_0(\boldsymbol{e}_x \pm \mathrm{i}\boldsymbol{e}_y) \,, \quad \boldsymbol{E}_{\mathrm{R}}^{\mp} = E_0(\boldsymbol{e}_x \mp \mathrm{i}\boldsymbol{e}_y) \,. \tag{1a}$$

The conjugate product $\boldsymbol{\Pi}^{\mathrm{A}}$ is negative to motion reversal T and positive to parity inversion P [14–16] and therefore has the same fundamental symmetries as magnetisation. Using perturbation theory [13] it can be shown that the effect exists both in paramagnetic and diamagnetic materials of chiral and achiral molecular symmetries. Pershan et al. [1–3], and Woźniak and co-workers [7–9] have shown that it is mediated by a similar type of the molecular property tensor [11] to the original, or forward, Faraday effect, which is circular dichroism due to static magnetic flux density. The inverse Faraday effect may therefore be thought of as the induction of a T negative, P positive molecular magnetic moment ($\boldsymbol{m}$) by the laser's conjugate product $\boldsymbol{\Pi}^{\mathrm{A}}$. Since $\boldsymbol{\Pi}^{\mathrm{A}}$ and $\boldsymbol{m}$ have the same T and P symmetries, it becomes clear that this induction must be mediated by a molecular property tensor which is itself T and P positive. It can be shown [14–16] that the induction of $\boldsymbol{m}$ by $\boldsymbol{\Pi}^{\mathrm{A}}$ also satisfies the Wigner principles of reversality and parity conservation [21, 22], which consequently allow the effect to occur in achiral ensembles such as water without P violation. This was demonstrated experimentally by Pershan et al. [2, 3]. The relation between the Faraday and inverse Faraday effect is seen particularly clearly through the fact that $\boldsymbol{\Pi}^{\mathrm{A}}$ has the same positive P and negative T symmetries as the static magnetic flux density $\boldsymbol{B}$. The same symmetry considerations have led recently [23, 24] to the inverse Zeeman effect and optical resonance effects akin to NMR and ESR.

The task of simulating the molecular dynamics associated with the induction of $\boldsymbol{m}$ by $\boldsymbol{\Pi}^{\mathrm{A}}$ is best described through the torque set up between the induced magnetic dipole moment $\boldsymbol{m}$ and the magnetic component $\boldsymbol{B}$ of the circularly polarised laser field. This is described in section 2. Other non-linear optical effects can be simulated with different types of torque. For example, inverse magnetochiral birefringence [13] is described in section 2 through the torque between $\boldsymbol{B}$ of the laser and the molecular magnetic dipole moment induced by a second type of conjugate product

$$\boldsymbol{\Pi}_2 = \boldsymbol{E}_{\mathrm{L}}^{+} \times \boldsymbol{B}_{\mathrm{L}}^{-} = \boldsymbol{E}_{\mathrm{R}}^{+} \times \boldsymbol{B}_{\mathrm{R}}^{-} = 2E_0 B_0 \boldsymbol{e}_z \,, \tag{2}$$

that of the inverse magnetochiral effect [13] introduced by Wagnière. The product $\boldsymbol{\Pi}_2$ differs in several important respects from the counterpart responsible for the inverse Faraday effect. Firstly, $\boldsymbol{\Pi}_2$ is negative to parity inversion P, while $\boldsymbol{\Pi}^{\mathrm{A}}$ is positive. This implies that inverse magnetochiral birefringence and dichroism is sustained in the absence of parity non-conservation only by chiral molecular symmetries. Secondly, $\boldsymbol{\Pi}_2$ is negative T [24], so that the molecular property tensor responsible for the induction of a molecular magnetic dipole moment by $\boldsymbol{\Pi}_2$ is T positive, P negative, and not T positive, P as in the inverse Faraday effect. Thirdly, $\boldsymbol{\Pi}_2$ is real while $\boldsymbol{\Pi}^{\mathrm{A}}$ is imaginary, so inverse magnetochiral birefringence requires the real, rather than imaginary, part of a mediating molecular property tensor [13]. (From semiclassical theory [25] molecular property tensors in general contain both real and imaginary parts, both in the presence and absence of resonance effects. The real part of the electronic molecular polarisability, for example, is T positive, P positive, and the imaginary part is T negative, P positive.)

"Dynamic polarisation" is described (section 2) through a torque generated by the electric component of the electromagnetic field and an induced electric dipole moment, $\boldsymbol{\mu}$, produced by the conjugate product $\boldsymbol{\Pi}^{A}$ [17, 26]. The induced electric dipole moment is T positive and P negative, whereas $\boldsymbol{\Pi}^{A}$ is T negative and P positive, and in consequence [17] induction of $\boldsymbol{\mu}$ by $\boldsymbol{\Pi}^{A}$ can be sustained only in chiral ensembles, through the T negative imaginary part of the molecular electronic hyperpolarisability. This rank three tensor, which is antisymmetric in the exchange of its last two subscripts, is non-zero in odd electron chiral molecules, or in atoms, where there is net electronic angular momentum. In the computer simulation of dynamic polarisation it is therefore necessary to use an electrically non-dipolar, chiral, odd electron molecule to isolate the effect of electric polarisation due to optical rectification from the strong first order torque generated between the permanent molecular electric dipole moment and $\boldsymbol{E}$ of the electromagnetic field.

Section 3 describes details of the molecular dynamics computer simulation of the dynamic polarisation; and section 4 is a detailed statistical analysis of the picosecond molecular dynamics of these non-linear optical effects in terms of a variety of time correlation functions. The latter may be divided into two broad categories, auto- and cross-correlations, both being used to characterise the effect of the laser on the ensemble molecular dynamics. Animation [27] has also been used during the course of this work to provide direct visual evidence of the molecular dynamics changes produced by the three types of torque. Section 5 is a description of the changes in the z component of the angular momentum autocorrelation function, where z is the propagation direction of the laser. This is proportional to the square of the ensemble averaged induced magnetic dipole moment, and is shown in section 5 to be particularly sensitive to small changes in the frequency of the applied laser in all three effects, thus signalling the presence of a previously unidentified type of laser frequency dependent, or dynamic, magnetisation. The latter originates in the phenomenon of electric polarisation due to optical rectification through the nonzero angular momentum imparted in the z (laser propagation) axis to the chiral molecular ensemble, for example by the spinning electric field vector part of the torque

$$\boldsymbol{T} = -\boldsymbol{\mu} \times \boldsymbol{E} \tag{3}$$

between the induced electric dipole moment and the electric part of the laser field. In the inverse Faraday effect it is due to the net angular momentum imparted by $\boldsymbol{B}$, the spinning magnetic component of the laser, through the torque

$$\boldsymbol{T}_2 = -\boldsymbol{m} \times \boldsymbol{B} \,, \tag{4}$$

where the induced magnetic dipole $\boldsymbol{m}$ is due to the conjugate product $\boldsymbol{\Pi}^{A}$. In the case of inverse magnetochiral birefringence, $\boldsymbol{\Pi}^{A}$ of the inverse Faraday effect has to be replaced by $\boldsymbol{\Pi}_2$.

The dynamic magnetisation manifests itself through the fact that the angular momentum z component autocorrelation function is nonzero as $t \rightarrow \infty$, where t is the time. This limiting value is proportional through the classical gyromagnetic ratio to $\langle m_z^{(d)} \rangle^2$, where $m_z^{(d)}$ is the induced dynamic molecular magnetic dipole moment. When the external laser frequency is tuned to the THz frequency scale (picosecond time scale accessible to the computer simulation), $\langle m_z^{(d)} \rangle^2$ becomes very sensitive to this frequency f, and is maximised at an optimum f. Details of this are given in section 4. Finally, a discussion section describes a possible experimental set-up for the observation of these effects.

2. The torques

The technique of field applied molecular dynamics computer simulation relies on a simple but useful modification of the forces loop of a standard molecular dynamics algorithm (of any type, [28]) to add in

the torque set up between an applied field of force and the appropriate molecular property (the arm of the torque). The technique was first introduced [29–32] for the interaction of a static electric field with a permanent molecular electric dipole moment. Here, the electric field is the force, and the dipole moment is the arm. In this context, the technique yielded new insight [29–32] to the dielectric relaxation and its high frequency adjunct, the far infrared [33] rise and fall transients, the Langevin and Kielich functions, the non-Markovian dynamics, the decoupling effects, the cross-correlation effects and a variety of other phenomena summarised in reviews [34, 35]. It was later extended to circularly polarised electromagnetic radiation [36–38] interacting with chiral and achiral molecular ensembles, and produced new insights summarised conveniently in a forthcoming long review, ref. [39]. In this case the arm was again a permanent electric dipole moment, but the externally applied force was the spinning electric field component of an electromagnetic plane wave.

Recently, Evans and Wagnière [17] have initiated the field applied simulation of non-linear optical effects. In this case, the arm is an *induced* dipole moment, which may be electric or magnetic. The induced dipole moment forms a torque with the electric or magnetic components of the electromagnetic field. Details of this torque have been given by Evans [26] and the effect has been animated [27] by the visualisation unit of Cornell Theory Center. The animation (on video) is available for general distribution [27] with descriptive sound track, and provides a direct visual description of the effects of the laser field [17] on 108 molecules of (S) bromochlorofluoromethane.

2.1. *Static electric polarisation due to optical rectification*

We consider a transparent isotropic medium composed of like molecules in which a left circularly polarised light wave (see eq. (A.1) in the appendix) with electric field

$$\boldsymbol{E}^{\mp} = E_0(\boldsymbol{e}_x \pm \mathrm{i}\boldsymbol{e}_y) \tag{5}$$

propagates in the z direction of the laboratory frame (x, y, z), inducing in each molecule the static electric dipole moment (see the appendix)

$$\mu_i = \beta'_{ijk}\Pi^{\mathrm{s}}_{jk} + \mathrm{i}\beta''_{ijk}\Pi^{\mathrm{A}}_{jk} \tag{6}$$

leading to the static electric polarisation

$$P_i = N[\langle \beta'_{ijk}\rangle \Pi^{\mathrm{s}}_{jk} + \mathrm{i}\langle \beta''_{ijk}\rangle \Pi^{\mathrm{A}}_{jk}], \tag{7}$$

where $\langle \ldots \rangle$ indicates a statistical average and N is the number of molecules per unit volume. The first term in eq. (7) vanishes after averaging because of symmetry with respect to permutation of the two last indices in β'_{ijk}, and we have

$$P_i = \frac{N}{6}\,\mathrm{i}\epsilon_{\alpha\beta\gamma}\,\beta''_{\alpha\beta\gamma}\Pi^{\mathrm{A}}_i\,, \tag{8}$$

with

$$\Pi^{\mathrm{A}}_i = \epsilon_{ijk}\Pi^{\mathrm{A}}_{jk}\,, \tag{9}$$

or in vector notation

$$\boldsymbol{\Pi}^{\mathrm{A}} = \boldsymbol{E}^{-} \times \boldsymbol{E}^{+}\,, \tag{10}$$

where $\epsilon_{\alpha\beta\gamma}$ is the Levi Civita third rank antisymmetric unit tensor. Using (A.9) of the appendix we have

$$\boldsymbol{P} = \frac{N}{3}\left(\beta''_{123} + \beta''_{231} + \beta''_{312}\right) \mathrm{i}(\boldsymbol{E}^- \times \boldsymbol{E}^+) \,. \tag{11}$$

For the optical wave (5)

$$\Pi^{\mathrm{A}} = \boldsymbol{E}^- \times \boldsymbol{E}^+ = -2\mathrm{i}E_0^2 \boldsymbol{e}_z \,, \tag{12}$$

and it follows that the electromagnetic radiation produces

$$P_z = \frac{N}{3}\left(\beta''_{123} + \beta''_{231} + \beta''_{312}\right) E_0^2 \,. \tag{13}$$

This shows that static electric polarisation can be induced by a circularly polarised laser in a system composed of chiral, odd electron molecules with a degenerate electronic ground state.

2.2. *Dynamic electric polarisation due to optical rectification*

In this section we describe dynamic polarisation due to the antisymmetric part of the product $E_j^- E_k^+$ only, i.e. due to Π_{jk}^{A} of the appendix. The real part of the induced electric dipole moment interacts with the real part of the electric field $\boldsymbol{E}^{\pm}$ to produce a torque on each molecule

$$\boldsymbol{T} = -\boldsymbol{\mu} \times \boldsymbol{E}^{\pm} \,, \tag{14}$$

with (see the appendix)

$$\mu_i = \mathrm{i}\beta''_{ijk} \Pi_{jk}^{\mathrm{A}} \,. \tag{15}$$

If the circularly polarised light propagates in the direction of the z axis of the laboratory frame of reference (x, y, z) (eq. (5)), then

$$\Pi_{jk}^{\mathrm{A}} = \mathrm{i}E_0^2 \begin{bmatrix} 0 & -1 & 0 \\ 1 & 0 & 0 \\ 0 & 0 & 0 \end{bmatrix} . \tag{16}$$

In the molecule fixed coordinate system (1, 2, 3)

$$\mu_\alpha = \mathrm{i}\beta''_{\alpha\beta\gamma} \Pi_{\beta\gamma}^{\mathrm{A}} \,, \tag{17}$$

where

$$\Pi_{\beta\gamma}^{\mathrm{A}} = e_{\beta j} e_{\gamma k} \Pi_{jk}^{\mathrm{A}} \,, \tag{18}$$

with $e_{\beta j}$ denoting the cosine of the angle between the β axis of the frame (1, 2, 3) and the j axis of (x, y, z). Using the purely geometric relations

$$\begin{cases} e_{2x}e_{3y} - e_{2y}e_{3x} = e_{1z} \,, \\ e_{3x}e_{1y} - e_{3y}e_{1x} = e_{2z} \,, \\ e_{1x}e_{2y} - e_{1y}e_{2x} = e_{3z} \,, \end{cases} \tag{19}$$

we have

$$\Pi^{A}_{\alpha\beta} = iE_0^2 \begin{bmatrix} 0 & -e_{3z} & e_{2z} \\ e_{3z} & 0 & -e_{1z} \\ -e_{2z} & e_{1z} & 0 \end{bmatrix} . \tag{20}$$

Taking into consideration (A.9) and (20) we have the induced electric dipole moment

$$\begin{cases} \mu_1 = 2e_{1z}\beta''_{123}E_0^2 , \\ \mu_2 = 2e_{2z}\beta''_{231}E_0^2 , \\ \mu_3 = 2e_{3z}\beta''_{312}E_0^2 , \end{cases} \tag{21}$$

and the torque

$$\begin{cases} T_1 = 2[e_{3z}\beta''_{312}\,\mathrm{Re}(E_2^{\pm}) - e_{2z}\beta''_{231}\,\mathrm{Re}(E_3^{\pm})] , \\ T_2 = 2[e_{1z}\beta''_{123}\,\mathrm{Re}(E_3^{\pm}) - e_{3z}\beta''_{312}\,\mathrm{Re}(E_1^{\pm})] , \\ T_3 = 2[e_{2z}\beta''_{231}\,\mathrm{Re}(E_1^{\pm}) - e_{1z}\beta''_{123}\,\mathrm{Re}(E_2^{\pm})] , \end{cases} \tag{22}$$

given in frame (1, 2, 3), with

$$\begin{bmatrix} E_1^{\pm} \\ E_2^{\pm} \\ E_3^{\pm} \end{bmatrix} = \begin{bmatrix} e_{1x} & e_{1y} & e_{1z} \\ e_{2x} & e_{2y} & e_{3z} \\ e_{3x} & e_{3y} & e_{3z} \end{bmatrix} \begin{bmatrix} E_x^{\pm} \\ E_y^{\pm} \\ 0 \end{bmatrix} . \tag{23}$$

The torque (23) is finally back-transformed into the laboratory frame (x, y, z) using the inverse transformation matrix of (23)

$$T_i = e_{i\alpha}T_{\alpha} . \tag{24}$$

The laboratory frame torque (24) is computed in the forces loop of a molecular dynamics algorithm at the point where the net intermolecular torque is calculated for each molecule, so that the total torque is the sum of the net torque on a given molecule due to other molecules plus the externally applied torque (24).

Note that the torque involves the imaginary part of a rank three electric hyperpolarisability tensor. In general, this has 27 elements. The work of Kielich, Woźniak, and co-workers [10, 40–42] reduces these to n independent elements, depending on the molecular point group symmetry. Since non-linear laser induced polarisation of this type necessarily deals with chiral symmetry, we restrict our attention to the chiral molecular point groups. In order to isolate effect 1 from strong first order effects (see the introduction) we must consider electrically nondipolar chiral point groups. An example is a two bladed propellor shaped molecule (see section 3) of point group D_2. In this point group there are three non-vanishing independent elements of the tensor $\beta''_{\alpha\beta\gamma}$ [10, 41].

The induced electric dipole moment in the molecule fixed frame can be expressed in terms of these independent elements as in eq. (21).

2.3. The inverse Faraday effect

The equivalent torque for the inverse Faraday effect is developed in much the same way, with important differences. Firstly, the inverse Faraday effect is sustained in both chiral and achiral molecular ensembles, paramagnetic and diamagnetic, indeed for all molecular point groups. Secondly, the torque of the inverse Faraday effect is

$$\boldsymbol{T}_2 = -\boldsymbol{m} \times \boldsymbol{B} \,, \tag{25}$$

where $\boldsymbol{m}$ is a magnetic dipole moment induced by the conjugate product ($\boldsymbol{\Pi}$) and $\boldsymbol{B}$ is the magnetic part of the electromagnetic plane wave, given in standard IUPAC notation by

$$\begin{aligned} \boldsymbol{B}_{\mathrm{L}}^{+} &= B_0(\boldsymbol{j} + \mathrm{i}\boldsymbol{i})\mathrm{e}^{\mathrm{i}\phi_{\mathrm{L}}} \,, \quad \boldsymbol{B}_{\mathrm{R}}^{+} = B_0(\boldsymbol{j} - \mathrm{i}\boldsymbol{i})\mathrm{e}^{\mathrm{i}\phi_{\mathrm{R}}} \,, \\ \boldsymbol{B}_{\mathrm{L}}^{-} &= B_0(\boldsymbol{j} - \mathrm{i}\boldsymbol{i})\mathrm{e}^{-\mathrm{i}\phi_{\mathrm{L}}} \,, \quad \boldsymbol{B}_{\mathrm{R}}^{-} = B_0(\boldsymbol{j} + \mathrm{i}\boldsymbol{i})\mathrm{e}^{-\mathrm{i}\phi_{\mathrm{R}}} \,. \end{aligned} \tag{26}$$

The induced magnetic dipole moment is given in general by

$$m_\alpha = (\boldsymbol{b}'_{\alpha\beta\gamma} + \mathrm{i}\boldsymbol{b}''_{\alpha\beta\gamma}) E_\beta E_\gamma \,, \tag{27}$$

where the tensor $\boldsymbol{b}''_{\alpha\beta\gamma}$ is T and P positive. The conjugate product (1) is the antisymmetric part of the general tensor product $E_\beta E_\gamma$. The symmetry properties of the rank three tensor $\boldsymbol{b}''_{\alpha\beta\gamma}$ have also been investigated for all the molecular point groups by the Kielich school [9–11]. For a chiral D_2 molecule, it has three independent elements, and $\boldsymbol{m}$ reduces to

$$\begin{cases} m_1 = 2E_0^2 e_{1z}\, b''_{123} \,, \\ m_2 = 2E_0^2 e_{2z}\, b''_{231} \,, \\ m_3 = 2E_0^2 e_{3z}\, b''_{312} \,, \end{cases} \tag{28}$$

in the molecule fixed frame of reference. In an achiral T_d symmetry spherical top, such as CCl_4, there is only one independent element of $\boldsymbol{b}''_{\alpha\beta\gamma}$, given by

$$b''_{123} = b''_{231} = b''_{312} = -b''_{213} = -b''_{132} = -b''_{321} \,, \tag{29}$$

and the molecule fixed frame torque of the inverse Faraday effect becomes

$$\begin{cases} m_1 = 2E_0^2 e_{1z} b''_{123} \,, \\ m_2 = 2E_0^2 e_{2z} b''_{123} \,, \\ m_3 = 2E_0^2 e_{3z} b''_{123} \,. \end{cases}$$

Finally, $\boldsymbol{B}$ is transformed into the molecule fixed frame, and the torque is transformed back into the laboratory frame as for effect 1.

2.4. Inverse magnetochiral birefringence

The torque is between the magnetic dipole moment induced by the conjugate product (2) and the spinning magnetic field of the electromagnetic plane wave

$$\boldsymbol{T} = -\boldsymbol{m} \times \boldsymbol{N} . \tag{31}$$

The induced magnetic dipole in the laboratory frame is, in general

$$m_i = b'_{1ijk} E_j B_k , \tag{32}$$

and the conjugate product (2) is the antisymmetric part of the tensor product $E_j B_k$. The product (2) is independent of circular polarisation [13] but is negative to T and P [24]. Inverse magnetochiral birefringence is mediated therefore by the real part of a molecular property tensor which is P negative and T positive.

It becomes clear, in summary, that the molecule fixed frame torques for these non-linear optical effects depend on elements of molecular property tensors. In general, these are unknown experimentally, but are increasingly accessible to ab initio computation [43, 44]. Quantum mechanical expressions for these elements are also available [13, 45] from perturbation theory, within whose framework resonance effects can be incorporated [45]. The torque therefore forms a useful link between quantum and classical approaches to non-linear optics and molecular dynamics.

3. Computer simulation method

Molecular dynamics computer simulation was used with a modified forces loop, in which the torque was supplemented, as described in section 2, with a component due to the applied external field. This modified molecular dynamics technique is well described in the literature [29–39]. The Cartesian components of the external torque are coded in to the forces loop at an instant t, and the sample allowed to regain equilibrium in the presence of the torque. This process involves several thousand time steps, which describe the rise transient, and Langevin and Kielich functions of various orders [29–32]. Re-equilibrium takes place through a thermostatting routine, which dissipates the rotational and translational kinetic energy (temperature increase) generated by the applied torque (the vector product of the external force and molecular arm). After completion of the re-equilibration process the ensemble is in "field-on equilibrium". In this condition, the molecular dynamics may be investigated visually by animation [27], and the sample is in a statistically stationary state, suitable for the computation of time correlation functions by running time averaging [29], over a minimum of six thousand time steps. Time correlation functions are generated out to a maximum of 400 time steps from the origin, $t = 0$, for good statistics. If the external torque is removed at the end of the field-on equilibrium interval, a fall transient is generated [34, 39]. Comparison of rise and fall transients produces information on the statistical nature of the molecular ensemble 34, 35].

The foregoing summarises the essential differences between our technique and standard molecular dynamics computer simulation.

3.1. Dynamic polarisation

Dynamic polarisation, as we have seen, requires an ensemble of chiral, paramagnetic molecules. Its isolation from first order effects requires that the molecule be electrically non-dipolar. To conform with these requirements, and to keep the consumption of supercomputer time to a reasonable minimum, we have selected the D_2 symmetry of bicyclopropene in a staggered conformation, with one ring at 45° to the other (a two bladed propeller). In this conformation, two enantiomers are generated. Each enantiomer was represented by six Lennard–Jones CH moieties, so that the total intermolecular potential was a six by six Lennard–Jones site–site potential with Lorentz–Berthelot combining rules

$$\epsilon/k(\mathrm{CH}) = 158.0\ \mathrm{K}; \quad \sigma(\mathrm{CH}) = 3.8\ \text{Å}\,. \tag{33}$$

The molecule can be represented more accurately by separate C and H Lennard–Jones sites, but at the expense of greatly increased computer time consumption. The paramagnetism was assumed to be generated by the π ring electrons, but clearly, the quantum nature of paramagnetism cannot be represented in a purely classical simulation, and our primary concern is to simulate the dynamic polarisation effect for a specific molecular point group, D_2, and to analyse the field on dynamics in terms of classical time correlation functions.

With this potential, and for a sample consisting of 108 molecules with periodic boundary conditions [34, 35, 39], a value of 1 ± 100 bar of pressure was generated at field off equilibrium for an input molar volume of $0.0014\ \mathrm{m}^3$; and an input temperature of 293 K. The large uncertainty in the pressure is characteristic of standard constant volume molecular dynamics simulation [35]. The potential energy [35, 39] of the sample in this condition was $-77\ \mathrm{kJ/mol}$.

"Baseline" time correlation functions were computed over three segments, each of 6000 time steps, at field free equilibrium for direct comparison with their counterparts at field on equilibrium. The correlation functions can be categorised generally as autocorrelation functions, of type

$$C_{\mathrm{auto}}(t) = \langle A_i(t) A_i(0) \rangle / \langle A^2(0) \rangle\,, \tag{34}$$

and cross-correlation functions, of type

$$C_{\mathrm{cross}}(t) = \langle A_i(t) A_j(0) \rangle / (\langle A_i^2 \rangle^{1/2} \langle A_j^2 \rangle^{1/2})\,, \tag{35}$$

or of type

$$C_{\mathrm{AB}}(t) = \langle A_i(t) B_j(0) \rangle / (\langle A_i^2 \rangle^{1/2} \langle B_j^2 \rangle^{1/2})\,, \tag{36}$$

where A and B denote two different molecular dynamical vectors. For example A may be the linear center of mass velocity and B the angular momentum. Note that most of these time correlation functions are damped out in about 400 time steps, so that running time averaging over 6000 time steps provides good statistics. The noise level may be judged from a baseline autocorrelation function such as that in fig. 1, showing three different Cartesian components of a nominally isotropic ensemble. (Thus, if there were no noise at all, these component autocorrelation functions would have an identical time evolution.) The time step was 0.005 ps (5 fs), and the correlation functions were computed using records separated by two time steps (0.01 ps) for several different molecular dynamical properties. The latter included: (i) the molecular angular momentum, proportional to the molecular magnetic dipole moment; (ii) the molecular orientation, described by unit vectors in the principal moment of the inertia frame; (iii) the time derivative of the orientation, known as the molecular rotational velocity, the Fourier transform of whose time correlation function is the far infrared power absorption coefficient [33]; (iv) the molecular center of mass linear velocity. Cross-correlation functions were constructed between the x and y components of these vectors at field on equilibrium.

The field on molecular dynamics were investigated visually with video animation in cooperation with the visualisation unit of Cornell Theory Center [27]. This animation is available for distribution from IBM, and is described briefly in section 4. Molecular dynamics data generating runs, thermodynamic analysis, and computation of correlation functions were carried out on the IBM 3090 supercomputer of ETH, Zurich. The graphical analysis was carried out on the mainframe computer of the University of Zurich, Irchel, and the animation analysis by satellite "sendfile" transmission to Cornell University, where "Wavefront" software was utilised on the Theory Center's IBM 3090-6S mainframe supercompu-

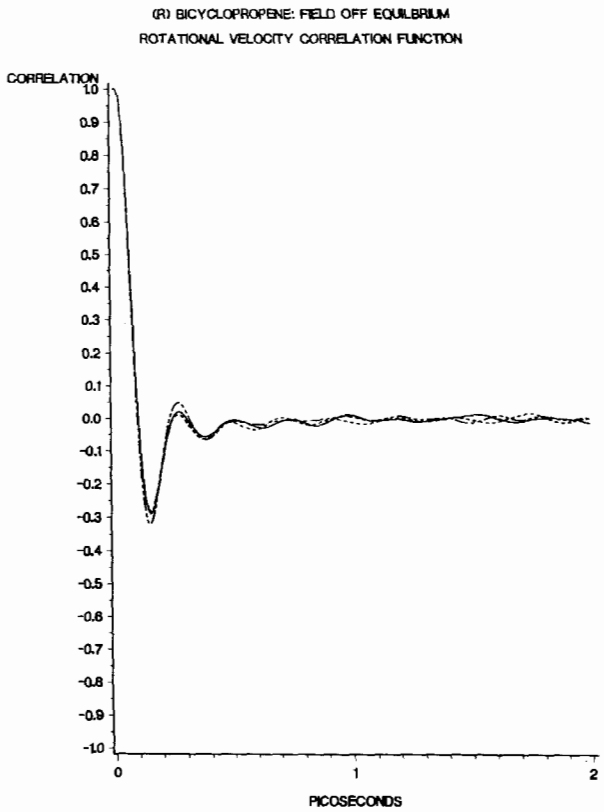

Fig. 1. Rotational velocity autocorrelation functions, laser-off equilibrium, Cartesian components computed over 6000 time steps each.

ter, IBM RISC 6000 workstation parallel processor network and homegrown animation apparatus, designed for this work by Mr. Chris R. Pelkie.

The runs completed at field on equilibrium are summarised in table 1 in terms of applied laser frequency (in THz) and the energy (in kJ per mole) imparted by the laser to the molecular ensemble. Experimentally these energy levels are accessible with contemporary picosecond of femtosecond mode locking laser technology [46–50]. In the absence of experimental and/or ab initio data for the mediating scalar elements of the torque, the following relative values were used

$$(\beta''_{123} - \beta''_{132}) : (\beta''_{231} - \beta''_{213}) : (\beta''_{312} - \beta''_{321}) = 1:2:3 . \tag{37}$$

3.2. *The inverse Faraday effect*

As far as the authors are aware, this is the first attempt at computer simulation of the inverse Faraday effect, which was stimulated for the two bladed propeller shaped molecule described already (staggered bicyclopropene). Some work was also completed for the T_d symmetry carbon tetrachloride molecule, and the C_{2v} symmetry water molecule, and will be reported fully elsewhere. The site–site potential for water [51, 52] was based on a modified ST2 [53–55]. Atom–atom interactions were modelled with Lennard–Jones and partial charge interactions, and the two lone pair electron sites with charge–charge interactions. This potential has been compared extensively with the ab initio water potentials of

Table 1
Potential energy (kJ/mol) vs. laser frequency in THz.

Potential energy	Frequency
−77	0
−55	1.7
−53	1.8
−63	2.0
−68	2.5
−71	3.0
	4.0
−59	10.0

Clementi and co-workers [56–61]. While no water potential has been devised that is capable of describing the complete range of available experimental data for water and the ices [62], our model is considered as satisfactory for our purpose, which is the investigation of the fundamental features of the molecular dynamics of the inverse Faraday effect in water. In this context, even if a "perfect" water potential existed, our simulation would still be constrained by lack of experimental and/or ab initio data on the tensor elements which are needed to define the torque (section 2). Indeed, there has been only one experimental investigation to date of the inverse Faraday effect [2, 3], despite the fact that it is a "textbook" phenomenon [5, 6]. There appear to be no ab initio computations to date of the molecular property tensor mediating the inverse Faraday effect. This can be accomplished in principle with contemporary software such as HONDO [63]. The following relative values of the scalar molecular property elements appearing in the torque were used for the three molecules

$$(b''_{123} - b''_{132}) : (b''_{231} - b''_{213}) : (b''_{312} - b''_{321}) = 1:2:3 \text{ (bicyclopropene)}, \tag{38}$$

$$(b''_{123} - b''_{132}) : (b''_{231} - b''_{213}) : (b''_{312} - b''_{321}) = 1:2:3 \text{ (water)}, \tag{39}$$

$$(b''_{123} - b''_{132}) : (b''_{231} - b''_{213}) : (b''_{312} - b''_{321}) = 1:1:1 \ (CCl_4). \tag{40}$$

The intermolecular potential for carbon tetrachloride was a Lennard–Jones five by five site–site model described in the literature [64, 65]. In this case there exists only one independent component in the torque (section 2).

At field off and field applied equilibrium, a set of auto- and cross-correlation functions was computed over segments of 6000 time steps for different laser frequencies and equivalent energies using 108 molecule ensembles for the three molecules. A wide variety of results was obtained, which were analysed graphically. The complete set of graphical data (several hundred correlation functions) is available on request, and the major results are described in section 4. The same time step of 5.0 fs was used throughout, and the time correlation functions built up using records of data every two time steps.

3.3. The inverse magnetochiral effect

This non-linear optical effect is sustained (section 2) only by chiral ensembles, and our two bladed propellor shaped molecule was used as a convenient model of a D_2 symmetry chiral molecule. (In this context it is also possible to use the lower (C_1) symmetry enantiomers and a racemic mixture of bromochlorofluoromethane [26, 66], whose molecular dynamics have also been animated [27, 67].) The same general methodology was used as for the other two non-linear optical effects, and results will be

fully discussed elsewhere for laser frequencies and imparted energies for 108 molecule samples over 6000 field-applied time steps. The field-applied molecular dynamics were analysed with sets of time correlation functions. The following relative values of scalar elements were used in computing the torque

$$(b'_{1,123} - b'_{1,132}) : (b'_{1,231} - b'_{1,213}) : (b'_{1,312} - b'_{1,321}) = 1:2:3 . \tag{41}$$

4. Results

4.1. Dynamic polarisation

The statistical analysis was carried out at up to twenty different laser frequencies in the range 30 to 3000 THz. At each frequency, correlation functions were evaluated in Cartesian components, each component representing a running time averaging over at least 6000 time steps. The complete data bank is available for distribution on request.

Animation analysis on the same trajectories (available for distribution on request) at Cornell Theory Center revealed that a major effect of the laser is to spin the molecular angular momentum vector about the propagation axis z. This sets up cross-correlation functions between the x and y components of the angular momentum. A typical result is given at five selected laser frequencies at constant intensity in fig. 2, which illustrates the function

$$C_J(t) = \frac{\langle J_i(t) J_j(0) \rangle}{\langle J_i^2 \rangle^{1/2} \langle J_j^2 \rangle^{1/2}} . \tag{42}$$

Time cross-correlation functions were also observed from the field applied statistical analysis for (i) the rotational velocity; (ii) the laboratory frame component x and y of the orientational unit vectors of the molecular principal moment of inertia coordinate frame. Much weaker cross-correlations were also observed for the center of mass linear velocity x and y components, showing that the rotational motion imposed by the circularly polarised laser is weakly correlated with the molecular center of mass translation [34, 35, 39].

Animation analysis showed that the rotational motion of the angular momentum vectors of each molecule of the ensemble is in competition with the background "Brownian" motion [33, 39] of the ensemble. For intense, high frequency applied laser pulses the imposed rotational motion dominates, and vice versa for weaker, lower frequency, pulses. The statistical effects corresponding to the animation are illustrated in fig. 3, which shows the behaviour of the z component angular momentum autocorrelation functions at five selected frequencies at constant laser intensity. Here, z is the laser propagation axis. The frequencies chosen are the same as those in fig. (2), and are compared with the "baseline" (field off) angular momentum time autocorrelation functions of z, y, and x laboratory frame components. It is clear from fig. (3) that the angular momentum correlation functions acquire a characteristic highly oscillatory pattern, and reach a significantly nonzero level as $t \rightarrow \infty$. This is proportional to the square of a dynamic magnetic dipole moment, $\langle m_z^{(d)} \rangle^2$. The value of $\langle m_z^{(d)} \rangle^2$ is strongly dependent on the applied laser frequency, f. This is discussed further in section 5. The x and y components of the field applied angular momentum autocorrelation functions under the same conditions are highly oscillatory about a zero $t \rightarrow \infty$ value. Both the oscillation patterns observed and oscillation amplitudes are critically dependent on the laser frequency, small changes in the latter produce large changes in the observed patterns. Animation analysis shows that for different laser frequencies and intensities, the laser induced rotational motion of the angular momentum vector about

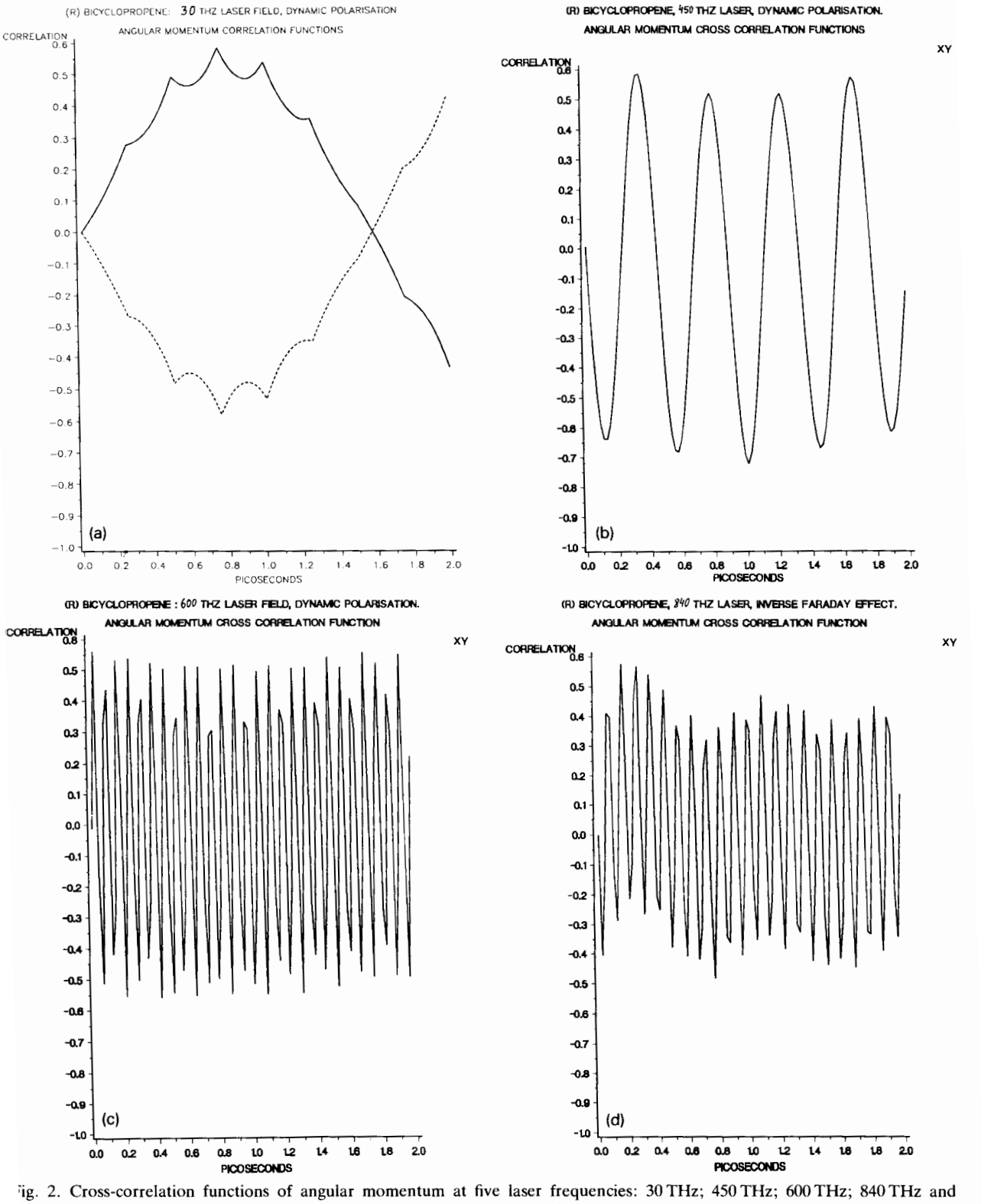

Fig. 2. Cross-correlation functions of angular momentum at five laser frequencies: 30 THz; 450 THz; 600 THz; 840 THz and 500 THz, as an illustrative sample of results available at 20 laser frequencies. The *xy* component is shown. The *yx* component is an accurate mirror image at each frequency.

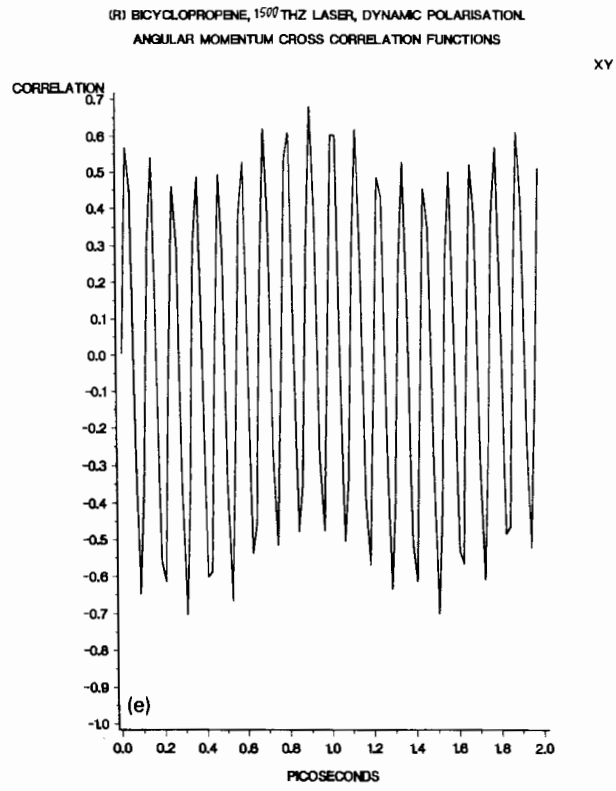

Fig. 2. (cont.)

the z axis may or may not dominate the background "Brownian motion" (which persists at field free equilibrium and which is represented, for example, by fig. 1). The two types of motion may or may not be clearly distinguishable by visual analysis alone, without recourse to statistical analysis at each laser frequency. The latter reveals (as sampled in figs. 2 and 3 a very rich variety of resultant behavior, which is extremely sensitive to small changes in laser frequency when the latter is tuned to the THz range.

The equivalent effect on the orientational autocorrelation functions is illustrated for the same small sample of five frequencies in fig. 4; and a sample of orientational cross-correlation functions between x and y components of orientation in fig. 5. The "baseline" orientational autocorrelation functions are also given in fig. 4, and the "baseline" (i.e. field off) orientational cross-correlation functions vanish for all t. The most characteristic features are (i) the development of strong orientational anisotropy; (ii) the development of x to y statistical cross-correlation, the xy and yx cross-correlation functions being mirror images. This anisotropy is accompanied by the development of nonzero second order orientational averages such as $\langle e_{iz}^2 \rangle$, where e_{iz} represents the z component of an orientational unit vector in any of the three principal moment of inertia axes of the molecule. Averages such as this were monitored over the 6000 time steps in the field applied condition. The clearly visible rotational motion of the angular momentum vectors of the 108 molecules in the animation does not work its way through to orientation (direct visualisation of molecular motion and interaction), so that although an animation of the motions of the molecules themselves reveals a visually discernible change in the dynamics as the laser is applied, correlation function analysis [27] is needed to probe further into the nature of these changes (figs. 1–5).

Of direct experimental interest is the dynamic polarisation effect of a laser on the rotational velocity time correlation function, which is defined as

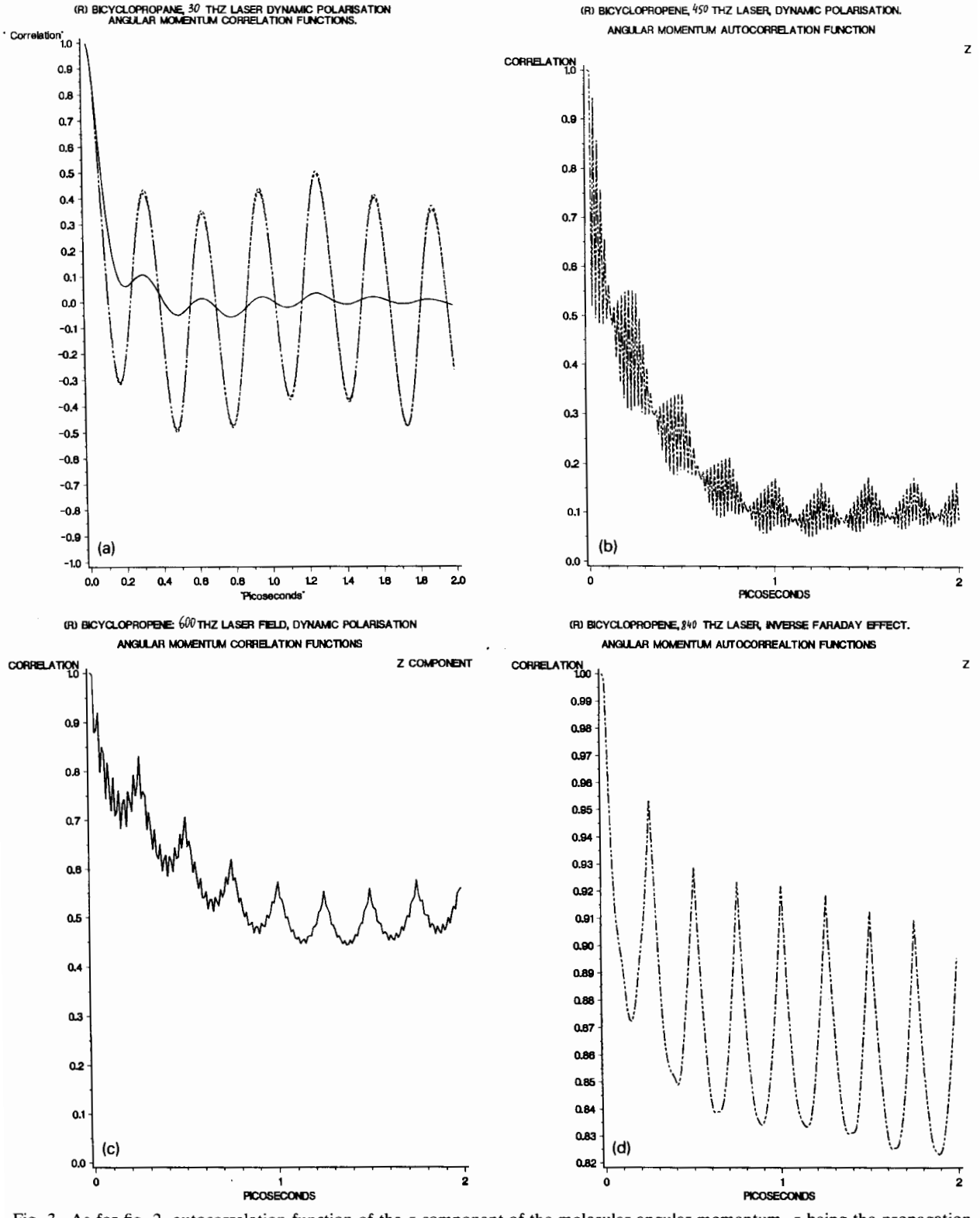

Fig. 3. As for fig. 2, autocorrelation function of the z component of the molecular angular momentum, z being the propagation axis of the laser.

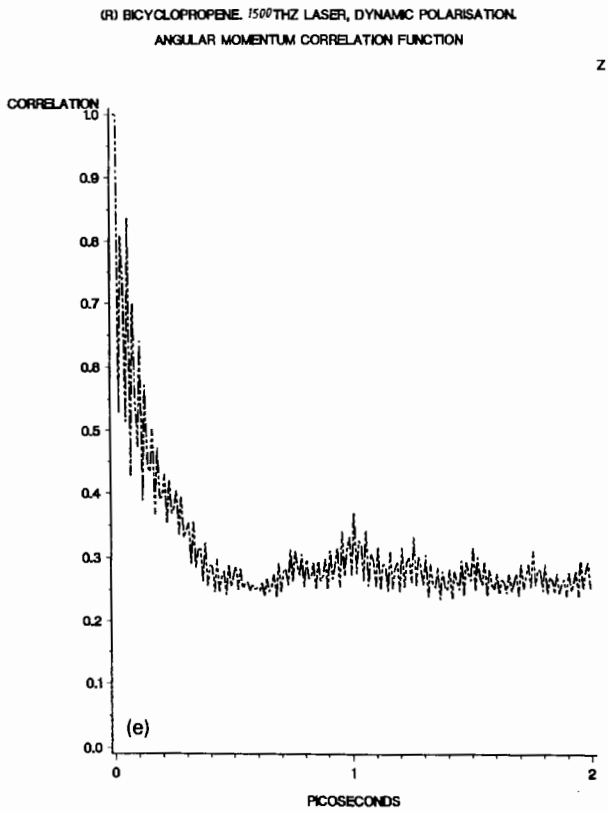

Fig. 3. (cont.)

$$C_{\mathrm{RV}}(t) = \frac{\langle \dot{e}_{1i}(t)\dot{e}_{1j}(0)\rangle}{\langle \dot{e}_{1i}^2\rangle^{1/2}\langle \dot{e}_{1j}^2\rangle^{1/2}}\,, \tag{43}$$

where e_1 is a unit vector in the principal moment of inertia axis 1 of the diffusing molecule, and $\dot{e}_1$ denotes its derivative with respect to time [33]. The Fourier transform of the rotational velocity autocorrelation function is proportional to the far infrared power absorption coefficient [33], which is directly observable by interferometric spectroscopy. Figures 6 and 7 show some of the characteristic oscillation patterns set up in the Cartesian components by the dynamic polarisation effect. The z component autocorrelation function is markedly different in time dependence from the other two (x and y component functions), but, unlike the angular momentum counterpart, does not attain a nonzero level as $t \rightarrow \infty$. Strongly oscillatory rotational velocity cross-correlation functions are shown in fig. 7, the xy and yx components being mirror images. The baseline (field off) correlation function is shown in fig. 1.

The statistical analysis of the rotational velocity in the dynamic polarisation effect is supported by an animation analysis, which shows a clearly visible spinning motion about z of the rotational velocity vectors of the 108 bicyclopropene molecules. The spinning becomes more or less prominent, depending on the laser frequency.

In summary, we have characterised the dynamic polarisation effect with a comprehensive set of correlation functions which forms the basis of our statistical analysis of the molecular dynamics. In general terms the anisotropy and oscillation frequency of the correlation patterns reveal an intricate

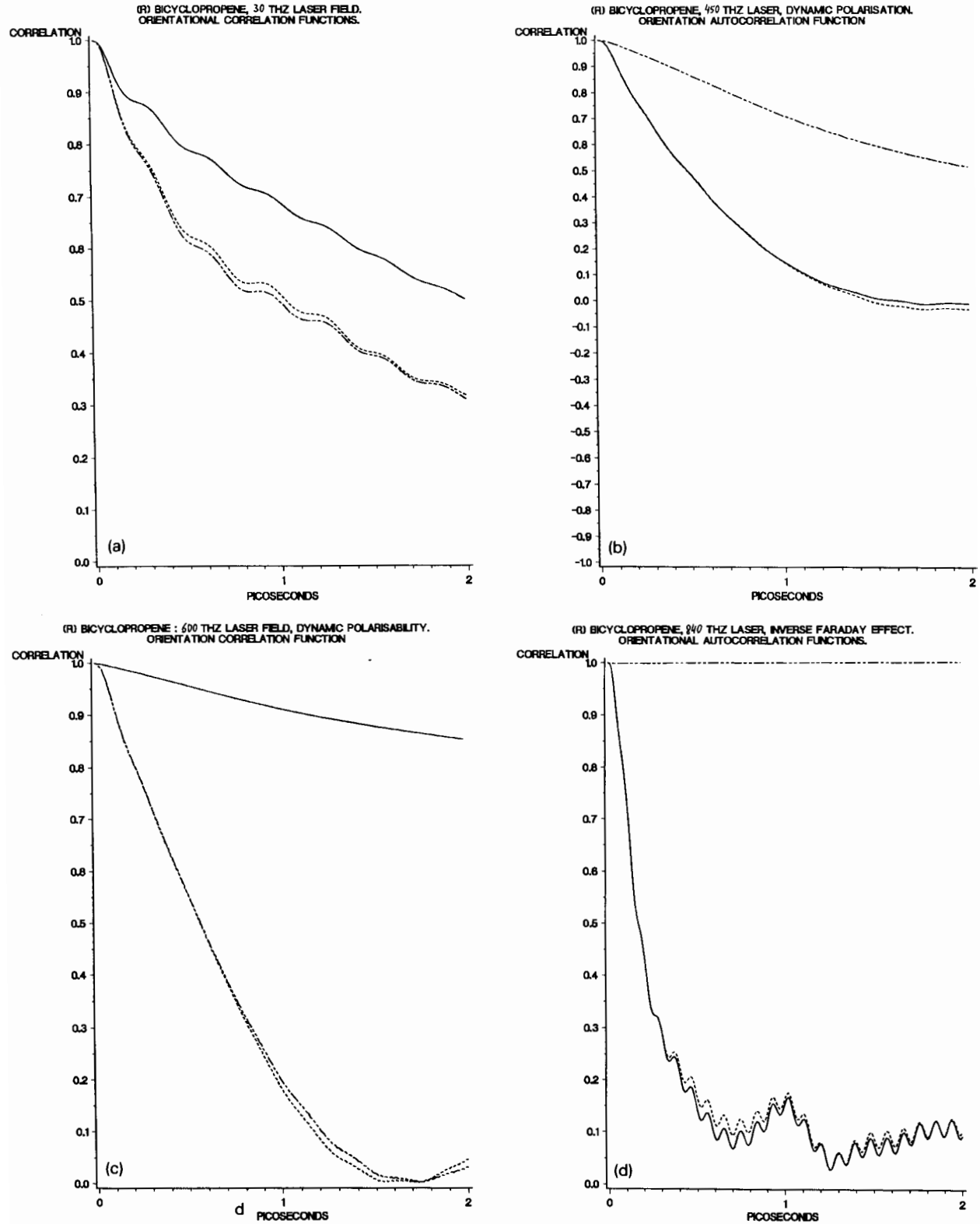

Fig. 4. As for fig. 2, the x, y and z components of the orientational autocorrelation functions at a sample of five laser frequencies.

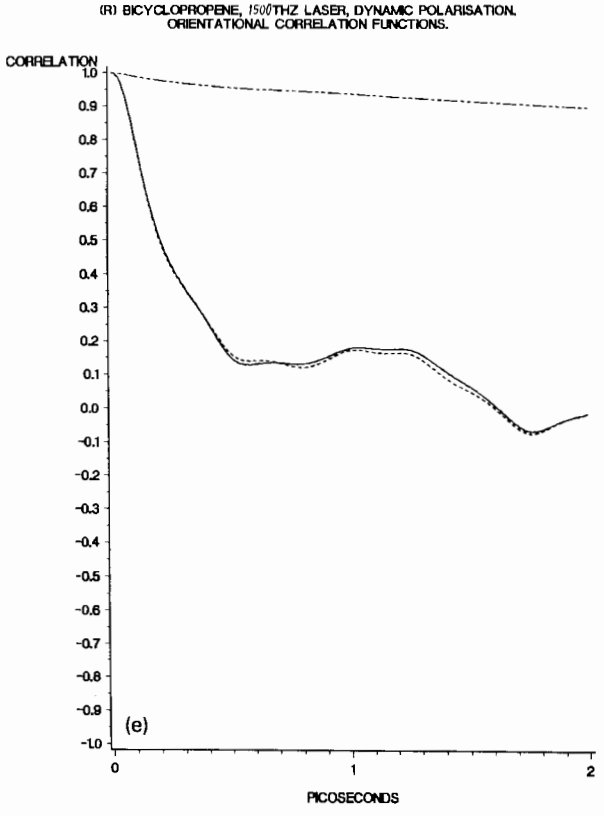

Fig. 4. (cont.)

dependence on the frequency of the laser. Similarly, the dynamic magnetisation shows maxima and minima (section 5) as a function of laser frequency for constant laser intensity and circular polarisation. Copious evidence has been gathered from statistical correlation analysis and animation for several novel aspects of the non-linear optical effect labelled "dynamic polarisation". The possible experimental observation of these effects is discussed later in this paper.

4.2. The inverse Faraday effect and the inverse magnetochiral birefringence

It is clear that the form of the torque for the inverse Faraday effect and inverse magnetochiral birefringence is numerically the same as that for the dynamic polarisation, so that it is possible to conclude immediately that the intricate pattern of molecular dynamics analysed in figs. 1 to 5 and generated by the laser will also be present in the inverse Faraday and magnetochiral effects. This will be discussed further elsewhere.

5. Dynamic magnetisation

The static and dynamic electric polarisation due to the conjugate product $\boldsymbol{\Pi}^{A}$ of the laser is accompanied by a hitherto uncharacterised effect of laser induced magnetisation which has been

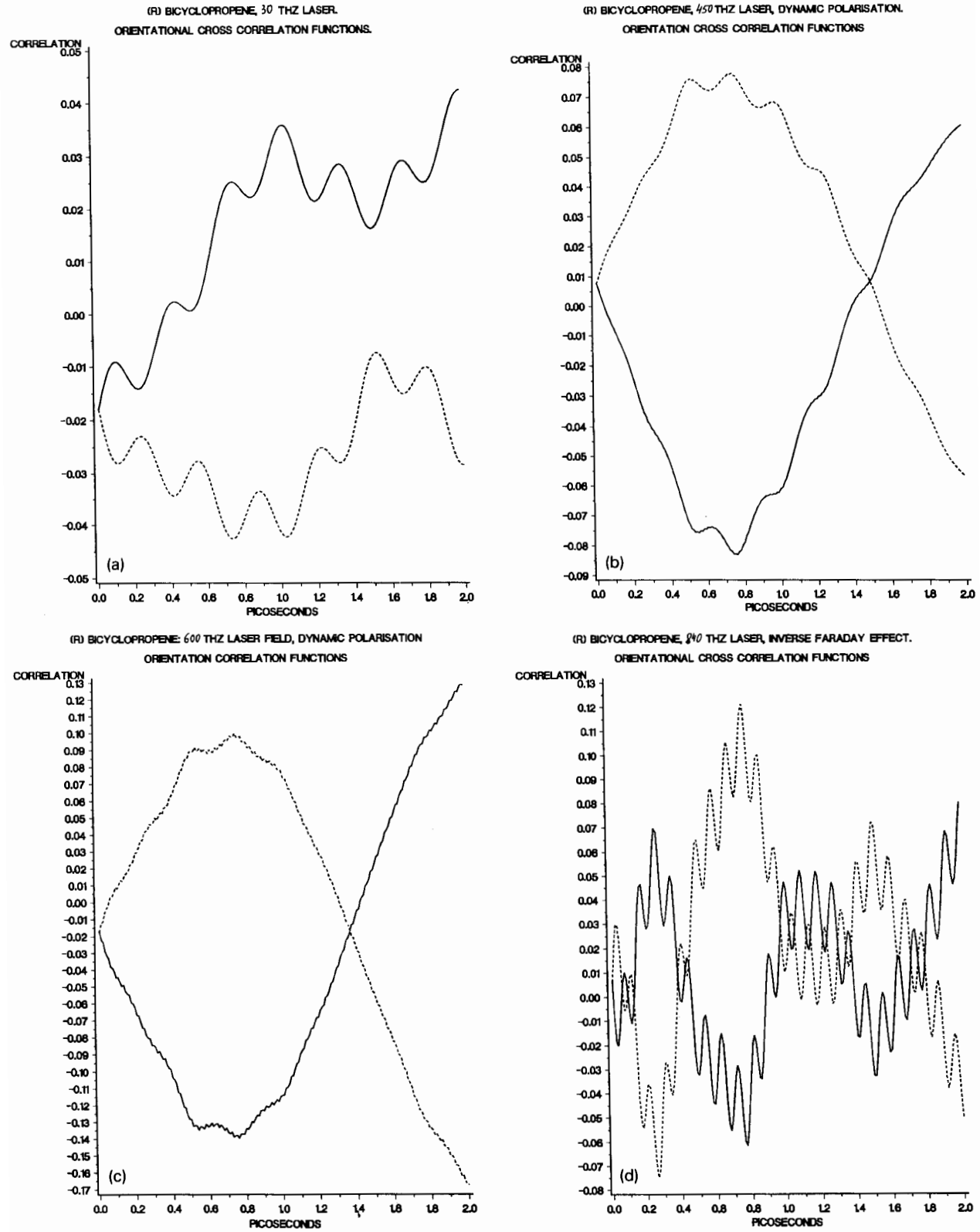

Fig. 5. As for fig. 2, a sample at five laser frequencies of the orientational cross-correlation functions induced by the conjugate product $\boldsymbol{\Pi}^{\wedge}$. Solid line is the xy component, dashed line is the yx. Note that the cross-correlation functions are accurate mirror images, and exhibit an intricate dependence on laser frequency.

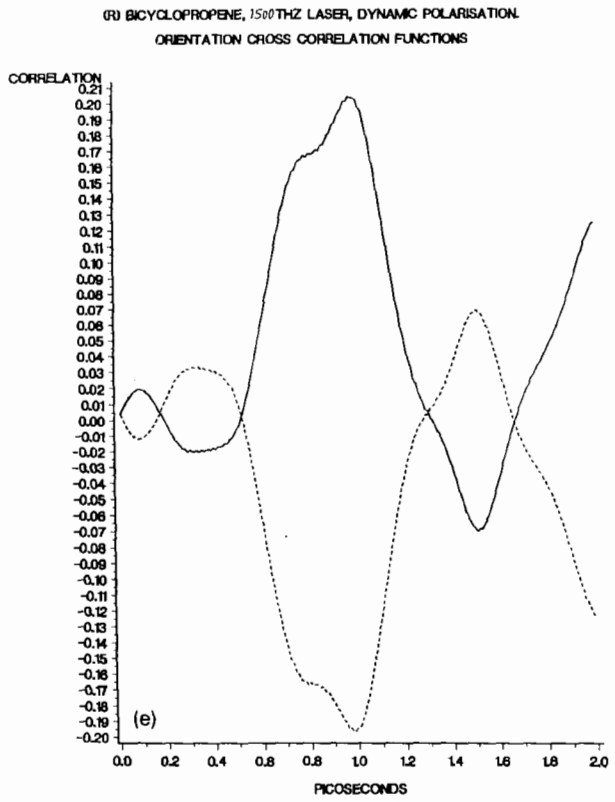

Fig. 5. (cont.)

isolated in this work by computer simulation. This is named "dynamic magnetisation", and is measured through the quantity $\langle m_z^{(d)} \rangle^2$ of section 4. Table 2 records the unitless dynamic magnetisation

$$m_{nz} = \langle m_z^{(d)} \rangle^2 / \langle m_z^2 \rangle \tag{44}$$

as a function of laser frequency in THz. The function m_{nz} has a complicated non-linear dependence on laser frequency (f), and a plot of it versus f in THz is a spectral function which can be used to characterise an odd electron chiral molecule in the dynamic polarisation effect, and, with broader applicability, to characterise both diamagnetic and paramagnetic molecules, chiral or achiral, in the inverse Faraday effect. Some simulations during the course of this work confirmed the presence of m_{nz} both in the inverse Faraday and inverse magnetochiral effects.

The complicated dependence of m_{nz} on frequency is easily understandable, in qualitative terms, by incorporating the torques of section 2 of this paper into a rotational Langevin equation [33], any analytical solution of which for the angular momentum correlation functions would be a complicated function of applied laser frequency. Such a Langevin equation is analytically insoluble, however, but may be accessible, in future work, to numerical solution. Experimentally, a result such as that recorded in table 2 appears to be potentially observable as a component in the frequency dependence of the magnetisation [1] of the inverse Faraday effect. In this eventuality, computer simulation would be a significant aid to interpretation. In some cases, as for the result of this section, computer simulation has revealed the presence of a phenomenon not previously characterised theoretically or experimentally,

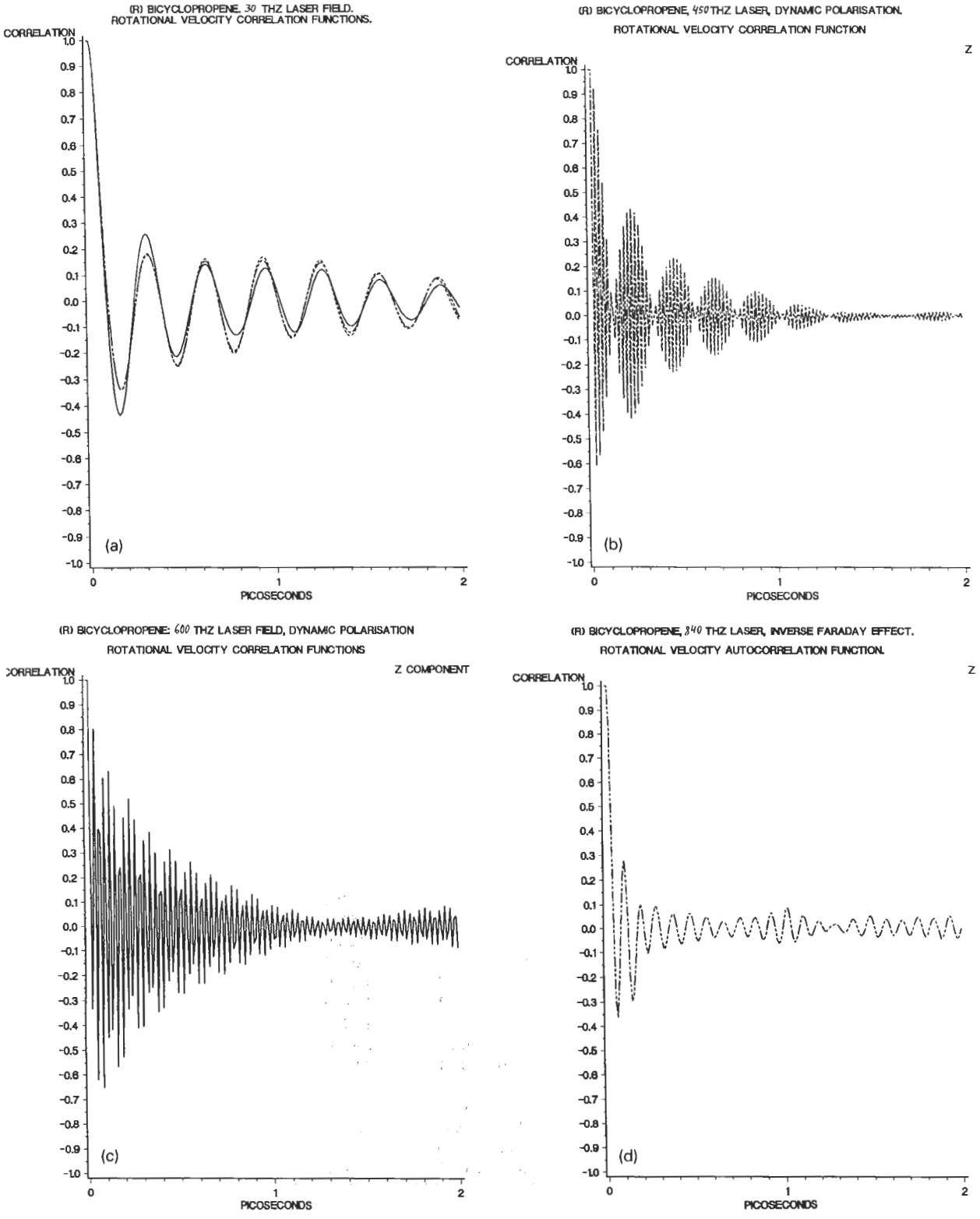

Fig. 6. As for fig. 2, the z component of the rotational velocity autocorrelation function.

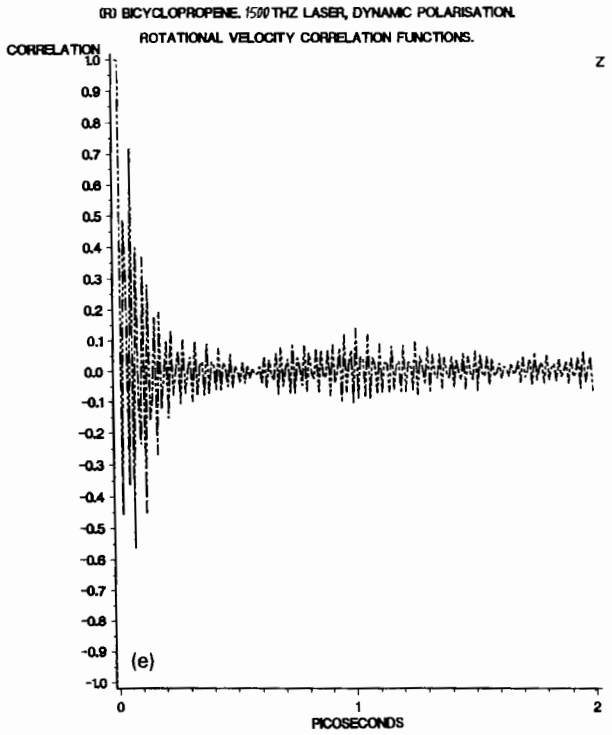

Fig. 6. (cont.)

Table 2
Magnetisation m_{n_z} vs. laser frequency.

Liquid	Normalised magnetisation	Laser frequency (THz)
S Bicyclopropene	0.002 ± 0.02	30.0
	0.025 ± 0.03	300.0
	0.10 ± 0.03	450.0
	0.55 ± 0.02	510.0
	0.67 ± 0.03	540.0
	0.54 ± 0.03	600.0
	0.79 ± 0.03	630.0
	0.76 ± 0.03	660.0
	0.80 ± 0.02	750.0
	0.87 ± 0.05	840.0
	0.80 ± 0.05	900.0
	0.88 ± 0.05	1020.0
	0.80 ± 0.02	1200.0
	0.65 ± 0.02	1350.0
	0.28 ± 0.02	1500.0
	0.00 ± 0.05	1800.0
	0.50 ± 0.02	2400.0
	0.90 ± 0.04	3000.0
Water	0.05 ± 0.05	300.0
	0.02 ± 0.07	500.0
	0.02 ± 0.06	600.0
	0.05 ± 0.03	1000.0

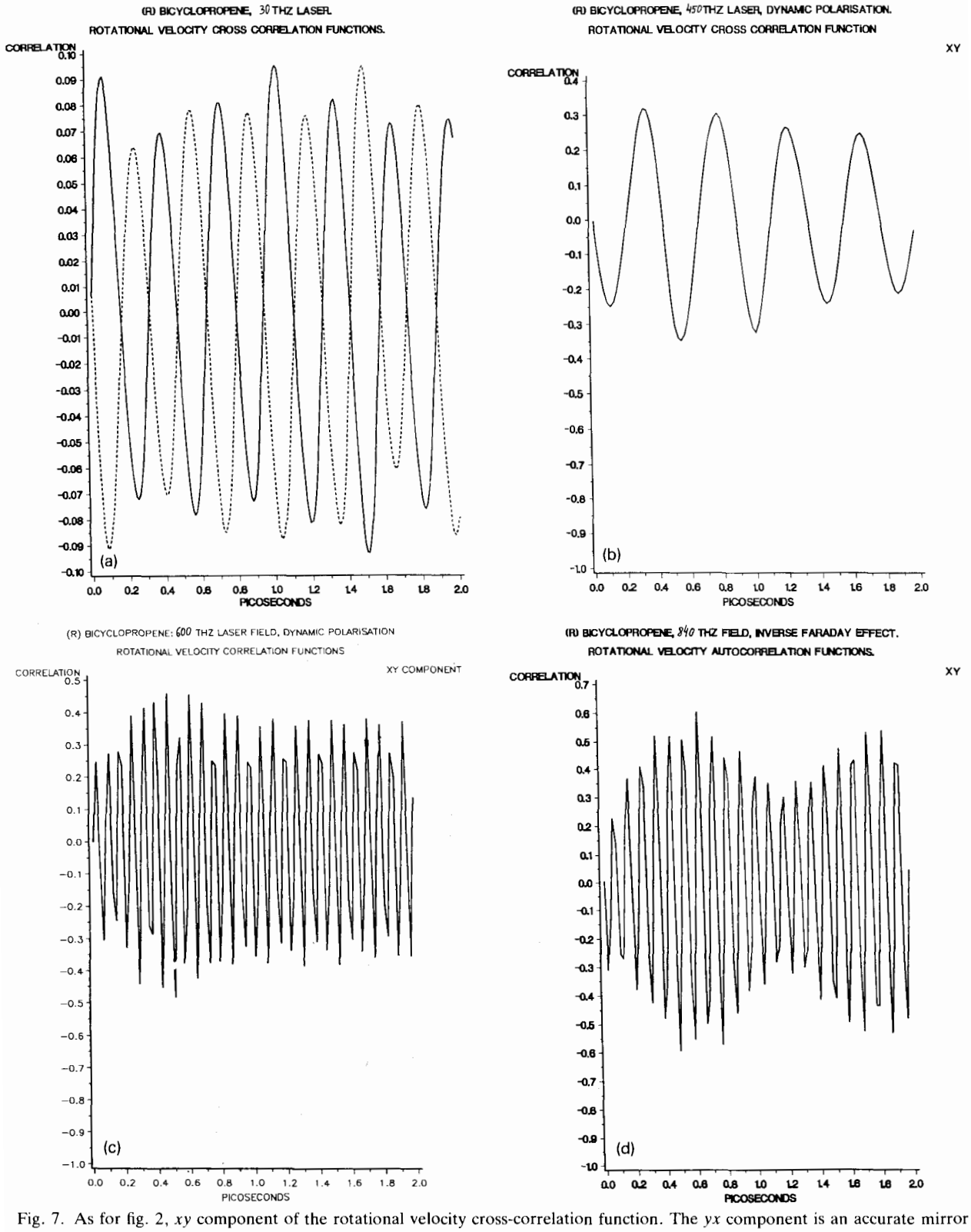

Fig. 7. As for fig. 2, *xy* component of the rotational velocity cross-correlation function. The *yx* component is an accurate mirror image at each frequency.

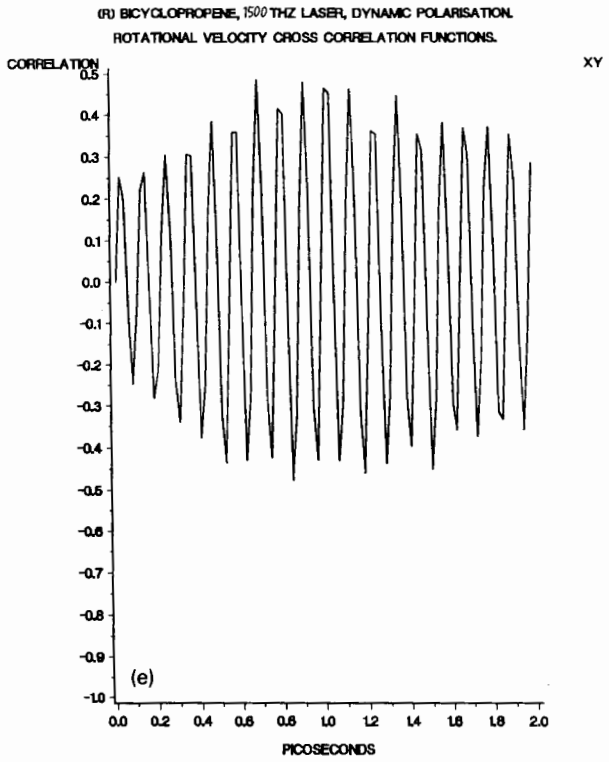

Fig. 7. (cont.)

but one which is easily understandable in terms of the competition between the angular momentum imparted to a molecule by the conjugate products of a laser, and the natural, or "Brownian" [33] molecular angular momentum.

6. Discussion

To observe static and dynamic electric polarisation due to the conjugate product of a pump laser, it is necessary to adapt the well developed techniques available [33–35] for the optical Kerr effect. These rely in general on pump and probe lasers. Static magnetisation due to the conjugate product $\boldsymbol{II}^{A}$ has been observed by Pershan et al. [1–3], and is the inverse Faraday effect. Static polarisation (eq. (13)) is observable in a much more restricted class of chiral, odd electron, molecules. The laser's conjugate product $\boldsymbol{II}^{A}$ also produces dynamic polarisation in this class of molecules, and dynamic magnetisation (section 5) in all types of molecules, because the latter accompanies the inverse Faraday effect as well as the dynamic polarisation effect.

In the computer simulation of this paper, it has been necessary to tune the pump laser to the THz range accessible to the picosecond time window of our rigid molecule simulation. In principle, there is no difficulty in using a pump laser at the carbon dioxide laser frequency, together with a model of the diffusing molecule which takes into account the intramolecular proper mode vibrations of the diffusing molecule. This would produce a great deal of insight into the dynamics of, for example, the inverse Faraday effect produced by an intense carbon dioxide laser at mid infrared frequencies.

Finally, a possible experimental approach to observing the picosecond scale molecular dynamics of a

variety of non-linear effects is that involving the use of a pump laser, followed at picosecond intervals by a probe. This method essentially monitors the fall transient [33–35] after the pump laser has interacted with the ensemble and has been switched off. The probe, arriving a few femto- or picoseconds later, measures the decay of the static or dynamic polarisation or magnetisation produced by the pump. In this case visible frequency pump and probe lasers can be used, as in the optical Kerr effect. Computer simulation can be used to interpret the experimental results from such an experiment. Such a procedure allows a check of the accuracy of the simulation, which can then be used to produce a data bank of information, and as in this paper, to try to detect the presence of previously uncharacterised phenomena. In this methodology, experimental data, simulation, and analytical theory are used in combination and in a complementary manner. The existing data on the inverse Faraday effect are confined to the original experiment by Van der Ziel et al. [2, 3] who used a pulse of giant ruby laser radiation of peak intensity $\sim 10^{11}$ W/m^2 to induce bulk magnetisation of 0.01 A/m in low temperature doped glasses and in room temperature diamagnetic liquids with high Verdet constants. It would be most interesting to extend this pioneering work and to investigate the frequency dependence of the magnetisation of the inverse Faraday effect and to investigate the dynamic polarisation of the current effect through band shape changes induced by the pump laser. These band shape changes are clearly present through the effect of the laser's conjugate product on time correlation functions such as the orientational and rotational velocity correlation functions of this paper.

We will pursue this investigation in future work in more detail, using the FMD simulation of second order rise transients induced in the inverse Faraday effect. These transients can be observed in principle with a minor modification of existing optical Kerr effect apparatus for use with a circularly polarised pump laser. With such apparatus it is possible to observe transients on a femtosecond scale, i.e. a time scale directly comparable with computer simulation.

Work closely related to the inverse Faraday effect is currently underway in the group of Professor W.S. Warren, Dept. of Chemistry, Princeton University. The experiment induces magnetisation in a contemporary NMR spectrometer with a circularly polarised laser.

Acknowledgements

MWE and SW thank the University of Zurich, and Professor Dr. Georges Wagnière for an invitation under the Swiss NSF Fellowship scheme. Part of this work (animation) was carried out at the Cornell Theory Center, which receives major funding from the US NSF, IBM (US), New York State, and the Corporate Research Institute. ETH Zurich is thanked for a major grant of computer time to MWE on the IBM 3090 joint facility of ETH and the University of Zurich. Dr. Laura J. Evans is thanked for invaluable help with the SAS plotting facilities of the University of Zurich, Irchel, local mainframe. Last but by no means least, Mr. Chris R. Pelkie is thanked for many hundreds of hours of animation analysis on the IBM 3090-6J supercomputer, RISC 6000 Model 530 work stations, and other computers of the Cornell National Supercomputer Facility, together with the meticulous preparation of the video animation cassette which is available on request from IBM.

Appendix

Matrix density formalism

An electric field

$$\boldsymbol{E} = \boldsymbol{E}^- \exp(-\mathrm{i}(\omega t - \boldsymbol{k}\cdot\boldsymbol{r})) + \boldsymbol{E}^+ \exp(\mathrm{i}(\omega t - \boldsymbol{k}\cdot\boldsymbol{r})) \tag{A.1}$$

of the electromagnetic wave induces in a molecule a static electric dipole moment (using the Einstein summation convention)

$$\mu_i = \beta_{ijk} E_j^- E_k^+ . \tag{A.2}$$

Matrix density formalism [68] produces

$$\beta_{ijk} = \beta'_{ijk} + i\beta''_{ijk} , \tag{A.3}$$

where

$$\begin{aligned}\beta'_{\alpha\beta\gamma} = \frac{1}{\hbar^2} \sum_{akl} \rho_{aa}^{(0)} \Bigg\{ & \frac{\mathrm{Re}[(\mu_\alpha)_{al}(\mu_\gamma)_{lk}(\mu_\beta)_{ka}]}{(\omega_{la} - i\Gamma_{la})(\omega_{ka} - \omega - i\Gamma_{ka})} \\ & + \frac{\mathrm{Re}[(\mu_\alpha)_{al}(\mu_\beta)_{lk}(\mu_\gamma)_{ka}]}{(\omega_{la} - i\Gamma_{la})(\omega_{ka} + \omega - i\Gamma_{ka})} + \frac{\mathrm{Re}[(\mu_\beta)_{al}(\mu_\gamma)_{lk}(\mu_\alpha)_{ka}]}{(\omega_{ka} + i\Gamma_{ka})(\omega_{la} + \omega + i\Gamma_{la})} \\ & + \frac{\mathrm{Re}[(\mu_\gamma)_{al}(\mu_\beta)_{lk}(\mu_\alpha)_{ka}]}{(\omega_{ka} + i\Gamma_{ka})(\omega_{la} - \omega + i\Gamma_{la})} + \frac{\mathrm{Re}[(\mu_\beta)_{al}(\mu_\alpha)_{lk}(\mu_\gamma)_{ka}](1+K)}{(\omega_{ka} + \omega - i\Gamma_{ka})(\omega_{la} + \omega + i\Gamma_{la})} \\ & + \frac{\mathrm{Re}[(\mu_\gamma)_{al}(\mu_\alpha)_{lk}(\mu_\beta)_{ka}](1+K)}{(\omega_{ka} - \omega - i\Gamma_{ka})(\omega_{la} - \omega + i\Gamma_{la})} \Bigg\} ,\end{aligned} \tag{A.4}$$

$$\begin{aligned}\beta''_{\alpha\beta\gamma} = \frac{1}{\hbar^2} \sum_{akl} \rho_{aa}^{(0)} \Bigg\{ & \frac{\mathrm{Im}[(\mu_\alpha)_{al}(\mu_\gamma)_{lk}(\mu_\beta)_{ka}]}{(\omega_{la} - i\Gamma_{la})(\omega_{ka} - \omega - i\Gamma_{ka})} + \frac{\mathrm{Im}[(\mu_\alpha)_{al}(\mu_\beta)_{lk}(\mu_\gamma)_{ka}]}{(\omega_{la} - i\Gamma_{la})(\omega_{ka} + \omega - i\Gamma_{ka})} \\ & + \frac{\mathrm{Im}[(\mu_\beta)_{al}(\mu_\gamma)_{lk}(\mu_\alpha)_{ka}]}{(\omega_{ka} + i\Gamma_{ka})(\omega_{la} + \omega + i\Gamma_{la})} + \frac{\mathrm{Im}[(\mu_\gamma)_{al}(\mu_\beta)_{lk}(\mu_\alpha)_{ka}]}{(\omega_{ka} + i\Gamma_{ka})(\omega_{la} - \omega + i\Gamma_{la})} \\ & + \frac{\mathrm{Im}[(\mu_\beta)_{al}(\mu_\alpha)_{lk}(\mu_\gamma)_{ka}](1+K)}{(\omega_{ka} + \omega - i\Gamma_{ka})(\omega_{la} + \omega + i\Gamma_{la})} + \frac{\mathrm{Im}[(\mu_\gamma)_{al}(\mu_\alpha)_{lk}(\mu_\beta)_{ka}](1+K)}{(\omega_{ka} - \omega - i\Gamma_{ka})(\omega_{la} - \omega + i\Gamma_{la})} \Bigg\} .\end{aligned} \tag{A.5}$$

Here $\boldsymbol{\mu}$ is an operator representing the electric dipole moment,

$$(\mu_\alpha)_{al} \equiv \langle a | \mu_\alpha | l \rangle$$

denotes an electric dipole transition between the states $|l\rangle$ and $\langle a|$,

$$\omega_{la} = \omega_l - \omega_a = (E_l - E_a)/\hbar ,$$

and $\rho_{aa}^{(0)}$ is the quantum mean value of the unperturbed density matrix in the stationary state $|a\rangle$. Γ_{la}^{-1} is a characteristic relaxation time between the states $|l\rangle$ and $|a\rangle$, whereas

$$K = i(\Gamma_{kl} - \Gamma_{ka} - \Gamma_{la})/(\omega_{kl} - i\Gamma_{kl}) \tag{A.6}$$

is the correction term, which can be ignored in other cases whenever the combination of damping terms in eq. (A.6) is small relative to the frequency ω_{kl} and which vanishes in the absence of damping, or if

$$\Gamma_{kl} = \Gamma_{ka} + \Gamma_{la} .$$

From (A.4) and (A.5) we have the following relation

$$\beta_{ijk} = \beta^{*}_{ikj} . \tag{A.7}$$

When absorption is neglected, we have the particular case

$$\beta'_{ijk} = \beta'_{ikj} , \tag{A.8}$$

$$\beta''_{ijk} = -\beta''_{ikj} , \tag{A.9}$$

and all components of the tensors $\boldsymbol{\beta}'$ and $\boldsymbol{\beta}''$ are real. Since $E^{-}_{j} E^{+}_{k}$ can be split into symmetric and antisymmetric parts

$$E^{-}_{j} E^{+}_{k} \equiv \Pi^{S}_{jk} + \Pi^{A}_{jk} , \tag{A.10}$$

with

$$\Pi^{S}_{jk} = \tfrac{1}{2}(E^{-}_{j} E^{+}_{k} + E^{-}_{k} E^{+}_{j}) , \tag{A.11}$$

$$\Pi^{A}_{jk} = \tfrac{1}{2}(E^{-}_{j} E^{+}_{k} - E^{-}_{k} E^{+}_{j}) , \tag{A.12}$$

Equation (A.2) can be written in the form

$$\mu_{i} = \beta'_{ijk} \Pi^{S}_{jk} + \mathrm{i}\beta''_{ijk} \Pi^{A}_{jk} . \tag{A.13}$$

The cross terms $\beta'_{ijk}\Pi^{A}_{jk}$ and $\beta''_{ijk}\Pi^{S}_{jk}$ vanish because of different symmetry with respect to permutation indices j and k in tensors $\boldsymbol{\beta}'$ and $\boldsymbol{\Pi}^{A}$ or $\boldsymbol{\beta}''$ and $\boldsymbol{\Pi}^{S}$. The hyperpolarisability β'_{ijk} (eq. (A.4)) exists in general for diamagnetic as well as paramagnetic (odd electron) molecules, but β''_{ijk} only for molecules with complex wave functions (eq. (A.5)).

References

[1] P.S. Pershan, Phys. Rev. 130 (1963) 919.
[2] J.P. van der Ziel, P.S. Pershan and L.D. Malmstrom, Phys. Rev. Lett. 15 (1965) 190.
[3] P.S. Pershan, J.P. van der Ziel and L.D. Malmstrom, Phys. Rev. 143 (1966) 574.
[4] P.W. Atkins and M.H. Miller, Mol. Phys. 15 (1968) 503.
[5] Y.R. Shen, The Principles of Non-Linear Optics (Wiley, New York, 1984).
[6] P.W. Atkins, Molecular Quantum Mechanics, 2nd Ed. (Oxford University Press, Oxford, 1982).
[7] S. Woźniak, Mol. Phys. 59 (1986) 421.
[8] S. Woźniak and R. Zawodny, Phys. Lett. A 85 (1981) 111; Acta Phys. Pol. A61 (1982) 175.
[9] S. Woźniak, B. Linder and R. Zawodny, J. de Phys. 44 (1983) 403.
[10] S. Kielich, Nonlinear Molecular Optics (Nauka, USSR, 1981).
[11] S. Woźniak, G. Wagnière and R. Zawodny, Phys. Lett. A 154 (1991) 259.
[12] G. Wagnière, J. Chem. Phys. 77 (1982) 2786.
[13] G. Wagnière, Phys. Rev. A 40 (1989) 2437.
[14] M.W. Evans, Phys. Rev. Lett. 64 (1990) 2909.
[15] M.W. Evans, J. Mod. Opt. 37 (1990) 1655.
[16] M.W. Evans, Spectrochim. Acta 46A (1990) 1475.
[17] M.W. Evans and G. Wagnière, Phys. Rev. A 42 (1990) 6732.

[18] M.W. Evans, Phys. Lett. A 149 (1990) 328.
[19] M.W. Evans and D.M. Heyes, Mol. Phys. 69 (1990) 241.
[20] M.W. Evans, Phys. Rev. A 39 (1989) 6041.
[21] L.D. Barron and J. Vrbancich, Mol. Phys. 51 (1984) 715.
[22] L.D. Barron, Chem. Soc. Rev. 15 (1986) 189.
[23] M.W. Evans, J. Mol. Spect. 143 (1990) 327.
[24] M.W. Evans, J. Phys. Chem. 95 (1991) 2256.
[25] L.D. Barron, Molecular Light Scattering and Optical Activity (Cambridge University Press, 1982).
[26] M.W. Evans, Phys. Rev. A 41 (1990) 4601.
[27] Animation by C.R. Pelkie of the Visualisation Unit of Cornell Theory Center, Cornell University, Ithaca, New York, 14853. USA. Video available for distribution, with narration. "Wavefront" software from data by M.W. Evans, IBM 3090-6S and RISC 6000 computer systems and specialised software/hardware.
[28] The method can be applied to any of the standard molecular dynamics algorithms in a library such as that of the CCP5 group of the Daresbury Laboratory of the Science and Engineering Research Council, near Warrington, WA4 4AD, UK.
[29] M.W. Evans, J. Chem. Phys. 76 (1982) 5473, 5480.
[30] M.W. Evans, J. Chem. Phys. 77 (1982) 4632.
[31] M.W. Evans, J. Chem. Phys. 78 (1983) 925.
[32] M.W. Evans, J. Chem. Phys. 79 (1983) 5403.
[33] M.W. Evans, G.J. Evans, W.T. Coffey, and P. Grigolini, Molecular Dynamics (Wiley Interscience, New York, 1982).
[34] M.W. Evans, in: Advances in Chemical Physics, Vol. 62, eds. M.W. Evans, P. Grigolini, G. Pastori-Parravicini, I. Prigogine and S.A. Rice (Wiley Interscience, New York, 1985) Ch. 5.
[35] M.W. Evans and G.J. Evans, in: Advances in Chemical Physics, Vol. 63, eds. M.W. Evans, I. Prigogine and S.A. Rice (Wiley Interscience, New York, 1985) Ch. 4.
D. Fincham and D.M. Heyes, in: Advances in Chemical Physics, Vol. 63, eds. M.W. Evans, I. Prigogine and S.A. Rice (Wiley Interscience, New York, 1985) Ch. 5.
[36] M.W. Evans, G.C. Lie and E. Clementi, J. Chem. Phys. 87 (1987) 6040.
[37] M.W. Evans, G.C. Lie and E. Clementi, Z. Phys. D 7 (1988) 397.
[38] M.W. Evans, G.C. Lie and E. Clementi, Phys. Lett. A 130 (1988) 289.
[39] M.W. Evans, in: Advances in Chemical Physics, Vol. 81, eds. I. Prigogine and S.A. Rice (Wiley Interscience, New York, 1991) in press.
[40] S. Woźniak and R. Zawodny, J. Chem. Phys. 84 (1986) 2566.
[41] S. Kielich, in: Dielectric and Related Molecular Processes, Vol. 1, M. Davies (senior rep.) (Chem. Soc., London, 1972).
[42] S. Kielich, Prog. Opt. 20 (1983) 155.
[43] E. Clementi, ed., MOTECC 89, (Escom, Leiden, 1989), with accompanying software package.
[44] E. Clementi, ed., MOTECC 90, (Escom, Leiden, 1990), with accompanying software package.
[45] S. Woźniak, work in progress.
[46] C. Reiser, J.I. Steinfeld and H.W. Galbraith, J. Chem. Phys. 74 (1981) 2189.
[47] D.C. Hanna, M.A. Yuratich and D. Cotter, Non-Linear Optics of Free Atoms and Molecules (Springer, New York, 1979).
[48] H.R. Gray and C.R. Stroud, Jr., Opt. Commun. 25 (1978) 359.
[49] W.A. Molander, C.R. Stroud, Jr. and J.A. Yeazell, J. Phys. 19 (1986) L461.
[50] S. Fenuille, Rep. Prog. Phys. 40 (1977) 1257.
[51] M.W. Evans, J. Mol. Liq. 32 (1986) 173.
[52] M.W. Evans, G.J. Evans, P. Minguzzi, C.J. Reid, G. Salvetti and J.K. Vij, J. Mol. Liq. 33 (1987) 279.
[53] M.W. Evans, J. Chem. Phys. 86 (1987) 4096.
[54] M.W. Evans, J. Mol. Liq. 34 (1987) 269.
[55] M.W. Evans, G.C. Lie and E. Clementi, Chem. Phys. Lett. 138 (1987) 149.
[56] M.W. Evans, G.C. Lie and E. Clementi, Phys. Rev. A 36 (1987) 226.
[57] M.W. Evans, G.C. Lie and E. Clementi, Phys. Rev. A 36 (1988) 3935.
[58] M.W. Evans, G.C. Lie and E. Clementi, Phys. Rev. A 37 (1988) 2551.
[59] M.W. Evans, G.C. Lie and E. Clementi, J. Chem. Phys. 88 (1988) 5157.
[60] M.W. Evans, G.C. Lie and E. Clementi, Phys. Rev. A 37 (1988) 2548.
[61] M.W. Evans, G.C. Lie and E. Clementi, J. Mol. Liq. 40 (1989) 285.
[62] G.H. Wagnière and J.B. Hutter, J. Opt. Soc. Am. B 6 (1989) 693.
[63] The software package HONDO is available for distribution and is described comprehensively in refs. [43] and [44] for a variety of molecular properties at various levels of ab initio approximation.
[64] M.W. Evans, Phys. Rev. A 35 (1987) 2989.
[65] M.W. Evans, K.N. Swamy, G.C. Lie and E. Clementi, Mol. Sim. 1, (1988) 187.

M.W. Evans, Phys. Rev. Lett. 50 (1983) 371.
The animation by C.R. Pelkie, from simulation data by M.W. Evans, shows the dynamic polarisation effect in an enantiomer of bromochlorofluoromethane for a variety of dynamical vectors such as angular momentum, torque, force rotational velocity, orientation; direct imaging of the dynamics of the 108 molecules with and without applied laser pulses; and scattegram analysis of time cross-correlation functions.
M. Weissbluth, Photon-Atom Interactons (Academic Press, London, 1989).